

# Supporting Information

## Unimolecular Photopolymerization of High-Emissive Materials on Cylindrical Self-Assemblies

*Liangliang Zhu,<sup>\*,†,§</sup> Xin Li,<sup>‡</sup> Samuel N. Sanders,<sup>§</sup> and Hans Ågren<sup>\*,‡</sup>*

L. Zhu

<sup>†</sup> State Key Laboratory of Molecular Engineering of Polymers, Department of Macromolecular Science, Fudan University, Shanghai 200433, China.

E-mail: zhuliangliang@fudan.edu.cn

Homepage: <http://www.polymer.fudan.edu.cn/polymer/research/zhull/>

X. Li, H. Ågren

<sup>‡</sup> Division of Theoretical Chemistry and Biology, School of Biotechnology, KTH Royal Institute of Technology, SE-10691 Stockholm, Sweden.

E-mail: agren@theochem.kth.se

L. Zhu, S. N. Sanders

<sup>§</sup> Department of Chemistry, Columbia University, New York, New York 10027, United States.

## Part I Experimental Section

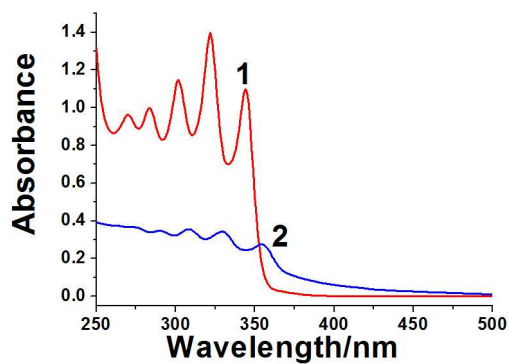


Figure S1. Absorption spectra of compound **1** (40  $\mu$ M, 298 K) in anhydrous THF (curve 1) and in THF with 90% water (curve 2).

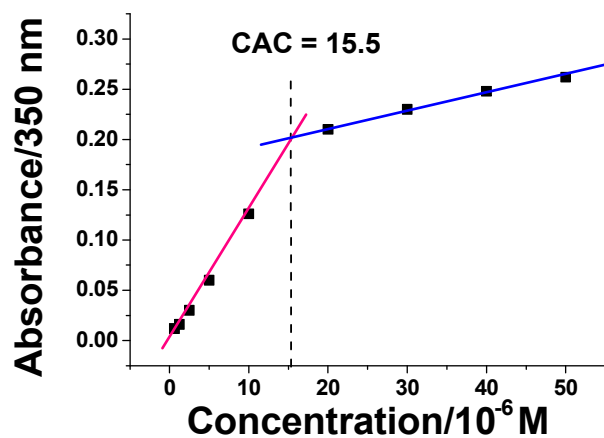


Figure S2. Dependence of the absorbance at 350 nm on the concentration of compound **1** (298K).

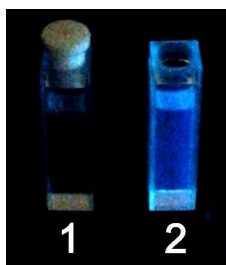


Figure S3. Photographs under a UV light of compound **1** in anhydrous THF (cuvette 1) and in THF with 90% water (cuvette 2).

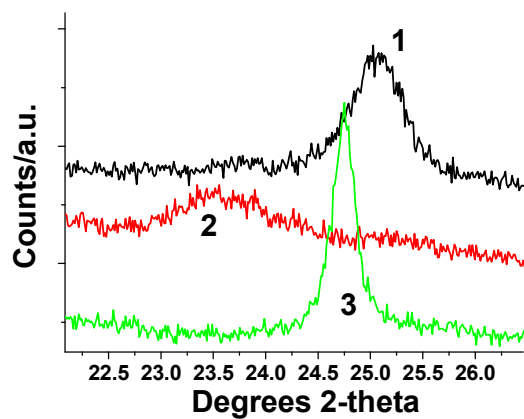


Figure S4. X-ray diffraction traces (curve 1-3) of the solid samples of compound **1**, **2** and **3**, respectively, dried from THF with 90% water.

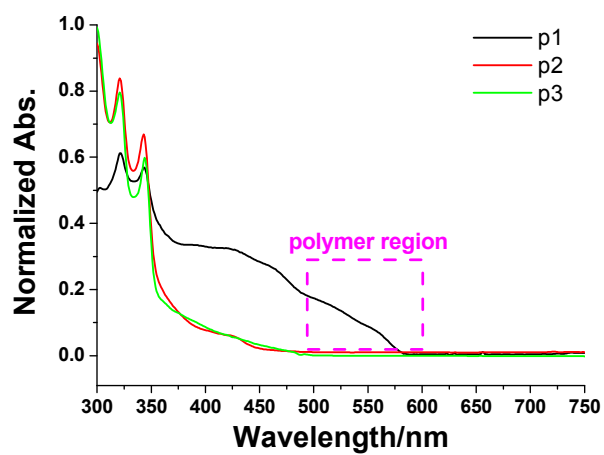


Figure S5. Absorption spectra of **1**, **2** and **3** after (curve p1-p3) UV-irradiation.

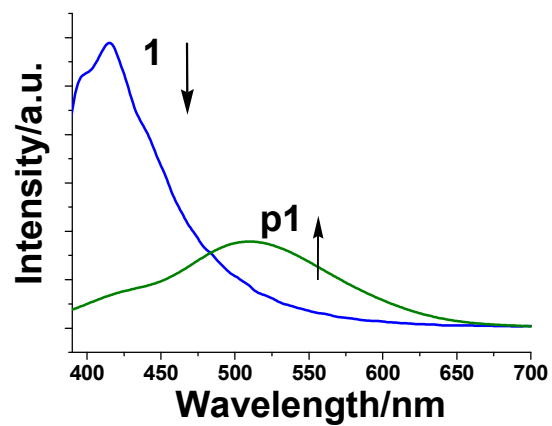


Figure S6. Emission spectra ( $\lambda_{\text{ex}} = 380 \text{ nm}$ ) of **1** ( $40 \mu\text{M}$ ,  $298 \text{ K}$ ) in THF with 90% water before (curve 1) and after (curve p1) UV-irradiation.

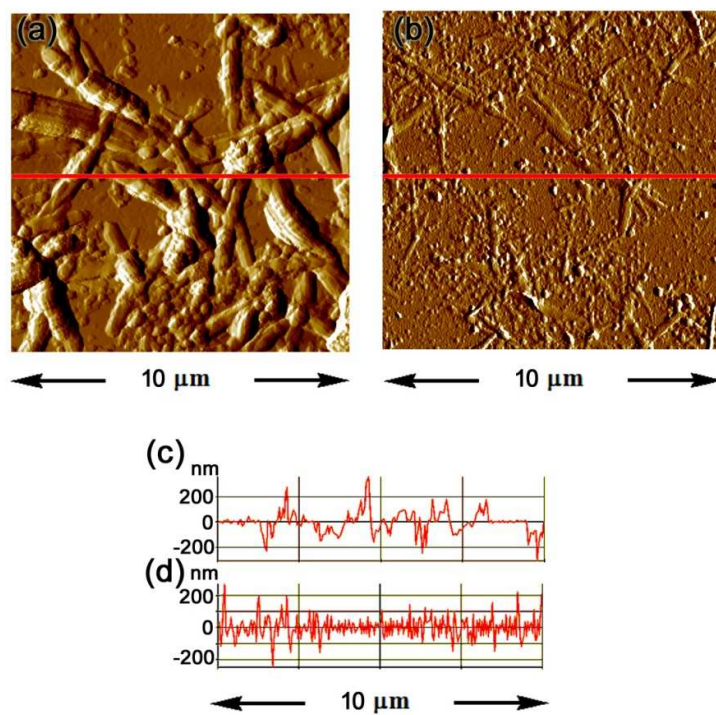


Figure S7. AFM images of **1** prepared from THF with 90% water (a) before and (b) after UV-irradiation. (c, d) Line height profiles of the image (a) and (b), respectively.

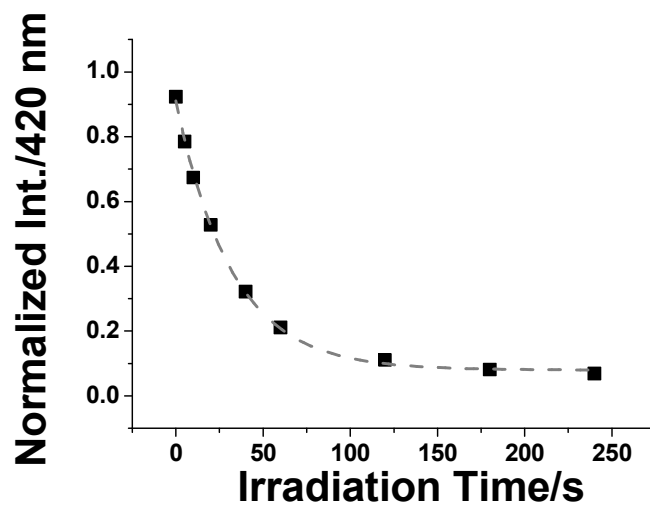


Figure S8. The normalized intensity changes of **1** (40  $\mu$ M, 298 K) in THF with 90% water monitored at 420 nm upon the prolonged UV-irradiation at 254 nm. The lines represent the data fitting according to first-order kinetic equations.

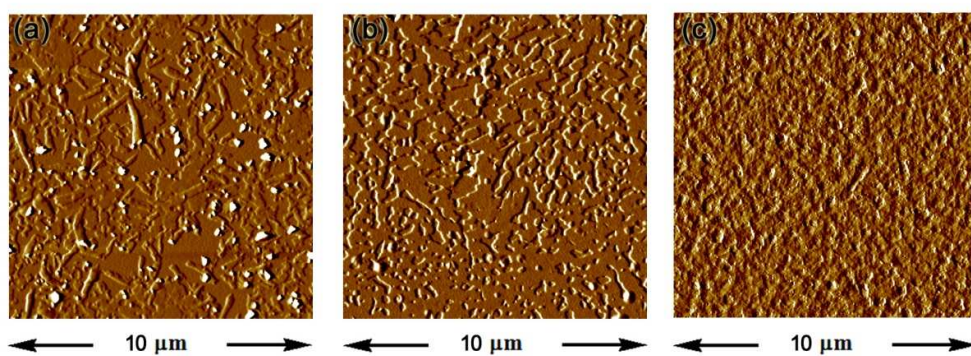


Figure S9. AFM images of the thin film samples of (a) **1**, (b) **2** and (c) **3**.

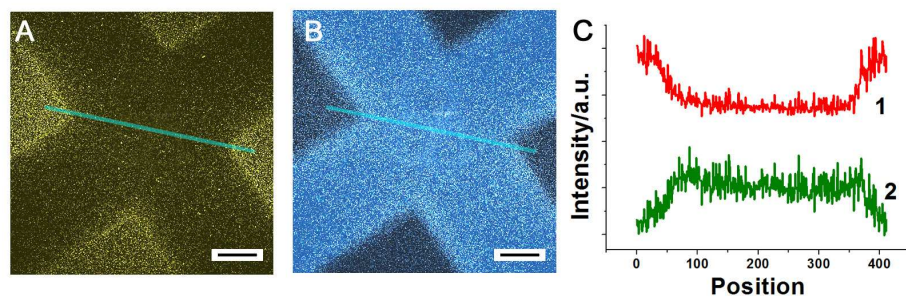


Figure S10. Magnified confocal luminescence images for the patterning film collected from the (A) FITC and (B) DAPI mode, respectively. Scale bar, 200  $\mu\text{m}$ . (C) (1,2) The intensity values of the both channels (corresponding to the images (A) and (B), respectively) along the line highlighted.

## Part II Computational Details

Density functional theory (DFT) calculations and time-dependent (TD) DFT calculations were carried out to investigate the electronic structure of the diphenyl-diacetylene core, using the Gaussian 09 program package.<sup>[S1]</sup> The B3LYP functional<sup>[S2]</sup> and the 6-31G(d) basis set<sup>[S3]</sup> were used to optimize the ground state structure, and the PBE0 functional<sup>[S4]</sup> and the 6-311++G(d,p) basis set<sup>[S5]</sup> were employed in subsequent TD-DFT calculations. Solvent effects of water were taken into account by the polarizable continuum model (PCM)<sup>[S6]</sup> in DFT and TD-DFT calculations. To gain insight into the aggregation behavior of the three compounds, we carried out molecular dynamics (MD) simulations in aqueous solutions. The general Amber force field (GAFF)<sup>[S7]</sup> was employed with partial atomic charges derived from the restrained electrostatic potential (RESP) fitting procedure.<sup>[S8]</sup> Here, the GAFF bonded parameters for bond lengths, bond angles and dihedral angles were refined to reproduce the quantum mechanically optimized geometries at the B3LYP/6-31G(d) level of theory.<sup>[S2,S3]</sup> Furthermore, additional dihedral angle parameters were added to correctly describe the rotational barrier between the two phenyl rings connected by the diacetylene group. For each compound, a 10-ns MD simulation was first carried out for one molecule in an aqueous solution. Then ten randomly distributed molecules were solvated by water molecules in a 10×10×10 nm<sup>3</sup> box and simulated under constant-*NpT* ensemble (*p* = 1 atm, *T* = 298 K) for 50 ns. The GROMACS program package<sup>[S9]</sup> was employed to carry out MD simulations. The results from molecular dynamics (MD) simulations was visualized by QuteMol.<sup>[S10]</sup>

To connect the self-assembling behavior of compound **1** and its AIEE nature, we examined the electronic structure of the diphenyl-diacetylene core by DFT and TD-DFT calculations. As shown in Table S1, the HOMO and LUMO are delocalized over the phenyl rings and the acetylene units, and TD-DFT calculations suggest that the HOMO→LUMO transition is allowed with a large oscillator strength of 1.504 (Table S2). Geometry optimization of the first excited singlet state suggests an emission wavelength at 444 nm (2.79 eV) with an oscillator strength of 1.880, comparable to the experimentally measured fluorescent wavelength. Upon rotation of the dihedral angle between the two phenyl rings to 90°, the  $\pi$ -conjugation of the whole molecule becomes twisted, and the electronic transitions between frontier molecular orbitals are prohibited, as reflected by the zero oscillator strengths (Table S2). Based on these findings it is inferred

that the AIEE of compound **1** likely follows the restricted intramolecular rotation (RIR) mechanism proposed by Tang and co-workers.<sup>[S11]</sup>

Table S1. Contour plots of frontier molecular orbitals of the diphenyl-diacetylene core under different dihedral angles, computed at the DFT/PBE0/6-311++G(d,p) level of theory.

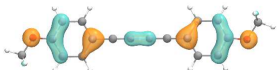
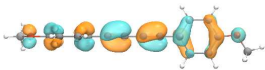
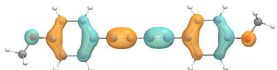
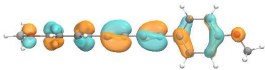
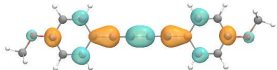
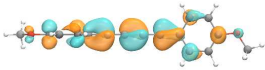
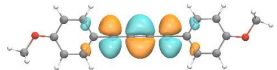
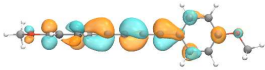
	$\varphi(\text{phenyl-phenyl}) = 0^\circ$	$\varphi(\text{phenyl-phenyl}) = 90^\circ$
HOMO-1		
HOMO		
LUMO		
LUMO+1		

Table S2. Low-lying excitation energies, oscillator strengths and molecular orbital compositions of the diphenyl-diacetylene core at different dihedral angles, computed at the TD-DFT/PBE0/6-311++G(d,p) level of theory.

	State	$\lambda_{\text{abs}}$	$f$	MO composition
$\varphi(\text{phenyl-phenyl}) = 0^\circ$	S <sub>1</sub>	3.47 eV, 357 nm	1.504	H → L (93%)
	S <sub>2</sub>	3.87 eV, 320 nm	0.000	H → L+1 (91%)
$\varphi(\text{phenyl-phenyl}) = 90^\circ$	S <sub>1</sub>	3.69 eV, 336 nm	0.000	H-1 → L (45%) H → L+1 (45%)
	S <sub>2</sub>	3.76 eV, 330 nm	0.000	H-1 → L+1 (46%) H → L (46%)
	S <sub>3</sub>	4.01 eV, 309 nm	0.001	H-1 → L (43%) H → L+1 (43%)



The aggregation characteristics of the three compounds were investigated by MD simulations. During the simulations we monitored the solvent-accessible surface area (SASA) of the self-assembled molecules, as shown in Figure S11. The SASA shows stepwise decrease with respect to simulation time, indicating gradual formation of the aggregation. At the beginning of the simulation, compound **2** has smaller SASA than **1** and similar SASA to **3**, which, however, becomes the largest at the end of the simulation trajectories. This suggests that the aggregation of compound **2** is the least efficient. The SASA of **1** is around 10 nm<sup>2</sup> larger than that of **3** at the beginning, and remains around 7 nm<sup>2</sup> larger than that of **3** at the end of simulations, reflecting that the compounds **1** and **3** exhibit similar degree of aggregation.

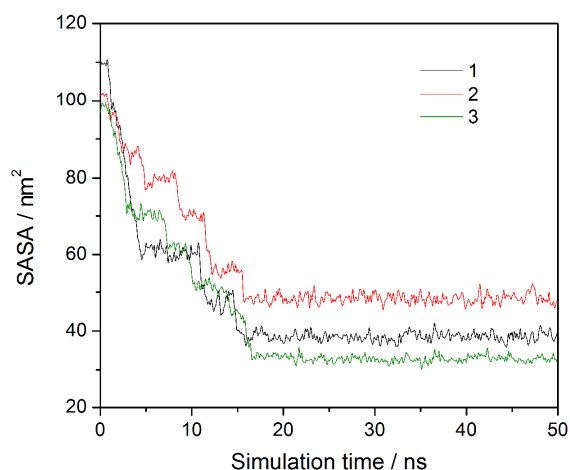


Figure S11. Solvent accessible surface area of the self-assembled molecules with respect to simulation time.

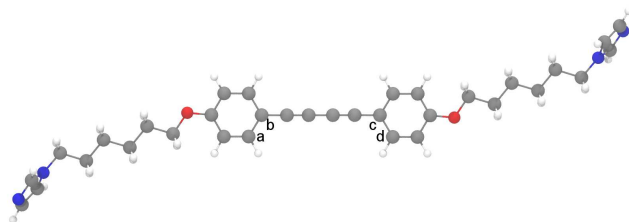


Figure S12. Optimized geometry of **1** at the DFT/B3LYP/6-31G\* level of theory.

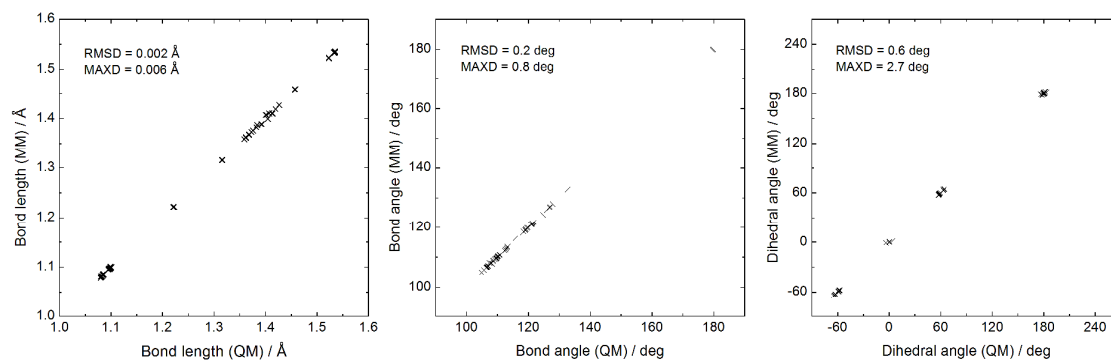


Figure S13. Comparison between the geometry of **1** optimized by quantum mechanical (QM) calculation at the DFT/B3LYP/6-31G\* level of theory and by molecular mechanical (MM) energy minimization using the refined GAFF parameters. The root mean square deviation (RMSD) and maximal deviation (MAXD) are also shown.

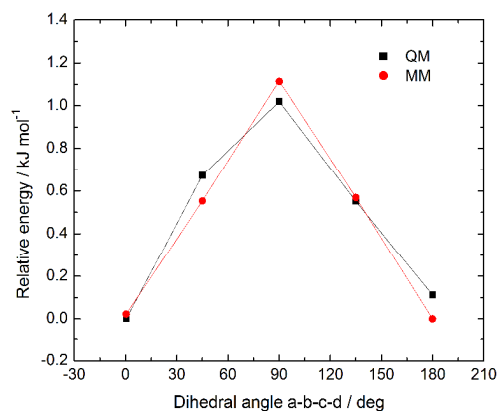


Figure S14. Comparison between the rotational barrier of dihedral angle a-b-c-d (see Figure S14) from QM and MM calculations.

## Reference

- [S1] Frisch, M. J.; Trucks, G. W.; Schlegel, H. B.; Scuseria, G. E.; Robb, M. A.; Cheeseman, J. R.; Scalmani, G.; Barone, V.; Mennucci, B.; Petersson, G. A.; et al. *Gaussian 09*, Revision A.02, Gaussian, Inc., Wallingford CT, **2009**.
- [S2] Becke, A. D. *J. Chem. Phys.* **1993**, *98*, 5648.
- [S3] Hehre, W. J. et al. *J. Chem. Phys.* **1972**, *56*, 2257.
- [S4] Perdew, J. P. et al. *Phys. Rev. Lett.* **1996**, *77*, 3865.

- [S5] Krishnan, R. et al. *J. Chem. Phys.* **1980**, 72, 650.
- [S6] Tomasi, J. et al. *Chem. Rev.* **2005**, 105, 2999.
- [S7] Wang, J. et al. *J. Comput. Chem.* **2004**, 25, 1157.
- [S8] Bayly, C. I. et al, *J. Phys. Chem.* **1993**, 97, 10269.
- [S9] Hess, B. et al. *J. Chem. Theory Comput.* **2008**, 4, 435.
- [S10] Tarini, M. et al. *IEEE Trans. Vis. Comput. Graph.* **2006**, 12, 1237.
- [S11] Luo, J.; Xie, Z.; Lam, J. W. Y.; Cheng, L.; Chen, H.; Qiu, C.; Kwok, H. S.; Zhan, X.; Liu, Y.; Zhu, D.; Tang, B.  
*Z. Chem. Commun.* **2001**, 1740.